PERGAMON

International Journal of Solids and Structures 36 (1999) 711–725

INTERNATIONAL JOURNAL OF SOLIDS and STRUCTURES

Mode I and mixed mode fields with incomplete crack tip plasticity

J. Li, J. W. Hancock*

Department of Mechanical Engineering, University of Glasgow, Scotland G12 8QQ, U.K.

Received 28 May 1997; in revised form 20 January 1998

Abstract

Plane strain slip line fields, in which plasticity does not fully surround the crack tip have been developed for mode I and mixed mode I/II cracks under contained yielding. Analytical solutions have been assembled using slip line theory for the plastic sectors and semi-infinite wedge solutions for the elastic sectors. These solutions are compared with finite element solutions based on modified boundary layer formulations. The analytical solutions agree well with numerical solutions, and form a family of fields with incomplete plasticity around the crack tip.

1. Introduction

Insight into the nature of plane strain elastic–plastic crack tip fields can be obtained by expressing the local crack tip deformation as plane slip line fields (Hill, 1950). For mode I deformation, Rice (1974) and Rice and Tracey (1974) have demonstrated the relevance of the Prandtl field, shown in Fig. 1, to small scale yielding. If plasticity surrounds the crack tip, the Prandtl field is the only possible non-trivial field which exhibits full continuity of tractions around the tip. The same field arises as an example of the dominant singularity solutions of Hutchinson (1968a, b) and Rice and Rosengren (1968) for power hardening materials in the limit of non-hardening plasticity. Although the HRR solutions describe the nature of the dominant singularity, higher order terms are now recognised to have an important effect on the constraint of plane strain crack tip fields (Betegón and Hancock, 1991; O'Dowd and Shih, 1991a, b). The HRR field is thus not the only possible crack tip field, but should be regarded as an important limiting case of a family of fields which arise when higher order terms are insignificant.

Interest is now focused on contained yielding, when local crack tip plasticity is completely contained within an outer elastic field. In these circumstances the level of constraint within the plastic zone depends on the nature of the non-singular terms in the outer elastic field. This field

* Corresponding author. Fax: 01413304343; e-mail: gnma18@mech.gla.ac.uk

0020–7683/99/$ - see front matter
PII: S0020–7683(98)00042–0

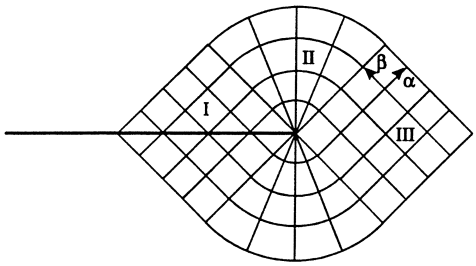

Fig. 1. The HRR mode I slip line field.

can be described as an asymptotic series using cylindrical coordinates (r, θ) centred at the crack tip following Williams (1959).

$$\sigma_{ij} = A_{ij}(\theta)r^{-1/2} + B_{ij}(\theta) + C_{ij}(\theta)r^{-1/2} + \cdots \tag{1}$$

The first term in the expression is singular at the crack tip whereas the remaining terms are finite and bounded. This allows the dominant elastic singularity to be characterized by the stress intensity factor.

$$\sigma_{ij} = \frac{K}{\sqrt{2\pi r}} f_{ij}(\theta) \tag{2}$$

In contrast, the second term is non-singular and corresponds to a uniaxial stress parallel to the crack which Rice (1974) has denoted the T stress.

$$\begin{bmatrix} \sigma_{11} & \sigma_{12} \\ \sigma_{21} & \sigma_{22} \end{bmatrix} = \frac{K}{\sqrt{2\pi r}} \begin{bmatrix} f_{11}(\theta) & f_{12}(\theta) \\ f_{21}(\theta) & f_{22}(\theta) \end{bmatrix} + \begin{bmatrix} T & 0 \\ 0 & 0 \end{bmatrix} \tag{3}$$

Larsson and Carlsson (1973) have demonstrated that the T stress has a significant effect on the shape of the crack tip plastic zone and the stresses within the plastic zone. Detailed investigations of the non-hardening problem have been presented by Du and Hancock (1991) using finite element analysis methods based on modified boundary layer formulations. As T is proportional to the applied load, the $T = 0$ field is significant in the sense that it is the field which applies at very small load levels for all geometries and is thus the small scale yielding field. In the non-hardening case, plasticity only encompasses the tip for closely defined conditions in which T is positive (tensile). When T is negative (compressive), plasticity does not surround the tip and an elastic sector appears on the crack flank giving rise to an incomplete Prandtl field. The possibility of fields with elastic sectors was first discussed by Nemat-Nasser and Obata (1984). In mode I a significant observation of Du and Hancock (1991), is that incomplete plasticity is associated with a compressive T stress and leads to a loss of crack tip constraint. Parallel experimental work has demonstrated that this leads to an enhanced level of toughness for both cleavage and ductile tearing. (Betegón and Hancock, 1991; Hancock et al., 1993; Kirk et al., 1993).

In mode II, the slip line field corresponding to the HRR singularity has been constructed by

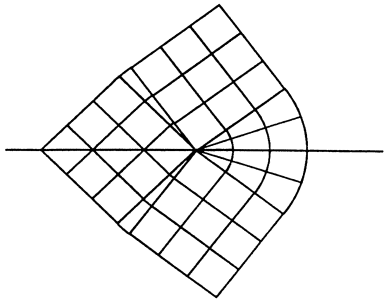

Fig. 2. The HRR mode II slip line field.

Hutchinson (1968b), and is shown in Fig. 2. Mixed mode I/II fields have been constructed by Shih (1974), on the assumption that plasticity entirely surrounds the crack tip. With the exception of near mode II fields, these require a discontinuity in radial stress in a sector trailing the crack front. In contrast Hancock et al. (1997) have discussed fields which differ from those constructed by Shih (1974) in that plasticity does not surround the crack tip and, with the exception of fields close to mode II field, an elastic wedge appears on the crack flanks.

The present paper constructs analytical solutions for mode I and mixed mode I/II fields in which plasticity does not surround the crack tip. Without loss of generality these fields are taken to comprise plastic and elastic sectors (Nemat-Nasser and Obata, 1984). The stresses within the elastic sectors are determined under incompressible deformation conditions by reference to solutions for a semi-infinite elastic wedge, while the plastic sectors are discussed in terms of plane strain slip line fields. Initially the structure of these sectors is discussed before sectors are assembled to give the complete analytical solutions. To verify these analytical solutions, numerical solutions have been obtained by using boundary layer formulations.

2. Analytical solutions

2.1. *Stress distribution in plastic sectors*

The stresses within plastic sectors at the crack tip can be conveniently represented by slip line fields as discussed by Rice (1974). The slip lines are the directions of maximum shear, on which the shear stress is the yield stress in shear, k. The value of k can be related to the uniaxial tensile stress σ_0 by the von Mises criterion $k = \sigma_0/\sqrt{3}$. In plane strain conditions the Mises yield criterion can be written in cylindrical co-ordinates, (r, θ) centred at the crack tip:

$$(\sigma_{\theta\theta} - \sigma_{rr})^2 + 4\sigma_{r\theta}^2 = 4k^2 \tag{4}$$

The assumption that the crack tip stresses are finite leads to the relationship:

$$r\frac{\partial \sigma_{ij}}{\partial r} \to 0 \quad \text{as } r \to 0 \tag{5}$$

This allows the equilibrium equations to be reduced to:

$$\frac{\partial \sigma_{r\theta}}{\partial \theta} + \sigma_{rr} - \sigma_{\theta\theta} = 0 \tag{6.1}$$

$$\frac{\partial \sigma_{\theta\theta}}{\partial \theta} + 2\sigma_{r\theta} = 0 \tag{6.2}$$

Differentiating the yield criteria, and combining with the reduced equilibrium equations (6.1) and (6.2) for incompressible deformation gives the relation identified by Rice (1974):

$$\frac{\partial \sigma_m}{\partial \theta} \cdot \frac{\partial \sigma_{r\theta}}{\partial \theta} = 0 \tag{7}$$

where σ_m denotes the mean stress. This leads to two possible forms, either:

$$\frac{\partial \sigma_m}{\partial \theta} = 0, \quad \frac{\partial \sigma_{r\theta}}{\partial \theta} \neq 0 \tag{8.1}$$

or,

$$\frac{\partial \sigma_{r\theta}}{\partial \theta} = 0, \quad \frac{\partial \sigma_m}{\partial \theta} \neq 0 \tag{8.2}$$

The first possibility, given by eqn (8.1), corresponds to sectors in which the mean stress (σ_m) does not change with angle, and the slip lines are straight corresponding to a constant stress sector. The second possibility corresponds to the situation in which the mean stress (σ_m) changes linearly with angle and is represented as a centred fan.

2.2. *Stress distribution in elastic sectors*

In all the cases discussed in the present work, elastic sectors lie on traction free crack flanks ($\theta = \pm\pi, \sigma_{r\theta} = \sigma_{\theta\theta} = 0$). The stress field within an elastic sector on a traction free crack flank can be expressed analytically by reference to the solution for a semi-infinite elastic wedge, loaded by constant surface tractions (Timoshenko and Goodier, 1970; Zywicz and Parks, 1992). It is now convenient to use two co-ordinate systems: θ is measured anticlockwise from a plane directly ahead of the crack and a right handed rule is used for stresses; γ is measured clockwise from the crack flanks so that $\gamma = \pi - \theta$ and a left handed rule is used for stresses as illustrated schematically in Fig. 3. Within the elastic wedge the stresses can now be written:

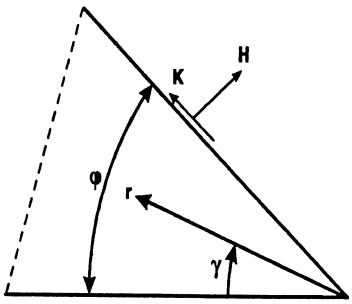

Fig. 3. An elastic wedge loaded by surface tractions H and K.

$$\sigma_{\theta\theta} = 2A(\cos 2\gamma - 1) + 2B(\sin 2\gamma - 2\gamma) \tag{9.1}$$

$$\sigma_{r\theta} = 2A \sin 2\gamma - 2B(\cos 2\gamma - 1) \tag{9.2}$$

$$\sigma_{rr} = -2A(\cos 2\gamma + 1) - 2B(2\gamma + \sin 2\gamma) \tag{9.3}$$

where

$$A = \frac{H(\cos 2\varphi - 1) + K(\sin 2\varphi - 2\varphi)}{4(1 - \cos 2\varphi - \varphi \sin 2\varphi)} \tag{10.1}$$

$$B = \frac{H \sin 2\varphi - K(\cos 2\varphi - 1)}{4(1 - \cos 2\varphi - \varphi \sin 2\varphi)} \tag{10.2}$$

Here H and K are the hoop or shear stresses on one side of the wedge as illustrated in Fig. 3, where A and B are constants. The angular span of the wedge is denoted φ.

2.3. *Assembly of the sectors*

Mode I. Guided by the form of the family of mode I slip line field discussed by Du and Hancock (1991) the sectors can now be assembled. The mode I symmetry condition requires that the slip lines cross the symmetry axis directly ahead of the crack at $\pm\pi/4$, corresponding to a constant stress sector. If continuity of stress is assumed, this sector must have a total angular span $\pi/2$, leading to a centred fan whose angular span is at the present time not determined. The equilibrium equations allow a jump in the radial stress but demand continuity of the hoop and shear stresses. The jump in radial stress can be determined from the allowable two roots of the plane strain yield criterion σ_{rr}^{+} and σ_{rr}^{-} (Shih, 1974). The allowable stress discontinuity is:

$$(\sigma_{rr}^{+} - \sigma_{rr}^{-}) = 4\sqrt{k^2 - \sigma_{r\theta}^2} \tag{11}$$

For a centred fan adjoining an elastic, or constant stress sector, $\sigma_{r\theta} = k$, there can thus be no stress jump, and full continuity of all the stress components is required. Compatibility conditions are satisfied across the boundary as both hoop and radial strains are zero for incompressible deformation in the two types of sector. In this case, K is, therefore, equal to the yield stress in shear, k, and the value of H can be obtained by equating the hoop stress and radial stress on the boundary from eqns (9.1) and (9.3):

$$H = \frac{2\varphi k \cos 2\varphi - k \sin 2\varphi}{1 - \cos 2\varphi} \tag{12.1}$$

$$K = k \tag{12.2}$$

The sectors can now be assembled by selecting a value for the angular span of the elastic wedge, φ. Equations (12.1)–(12.2) define the constants H and K, which can be used in equations (9.1)–(9.3).

The stresses in the plastic sectors can be obtained from the Hencky equations (Hill, 1950), which are the equations of equilibrium referred to the curvi-linear slip lines. The stresses within the fan can be expressed in terms of the angular span of the elastic sector (φ) and the hoop stress (H) on the boundary between fan and elastic sector as shown in Fig. 3.

$$\sigma_{\theta\theta} = \sigma_{rr} = \sigma_{zz} = \sigma_m = 2k(\pi - \varphi - \theta) - H \tag{13.1}$$

$$\sigma_{r\theta} = k \tag{13.2}$$

The stresses within the constant stress sector are:

$$\sigma_{\theta\theta} = k(\cos 2\theta - 2\varphi + \tfrac{3}{2}\pi) - H \tag{14.1}$$

$$\sigma_{rr} = k(-\cos 2\theta - 2\varphi + \tfrac{3}{2}\pi) - H \tag{14.2}$$

$$\sigma_{r\theta} = k \sin 2\theta \tag{14.3}$$

$$\sigma_{zz} = \sigma_m = k(\tfrac{3}{2}\pi - 2\varphi) - H \tag{14.4}$$

These solutions are valid in the range $\pi/4 \leqslant \varphi \leqslant 3\pi/4$. Outside this range, the yield criterion is violated in any postulated elastic sector.

Alternatively, the sectors can be assembled by selecting a value of the constraint parameter, Q. Following O'Dowd and Shih (1991), the stress fields can be characterised by a constraint parameter, Q:

$$\sigma_m = \sigma_m^{\mathrm{SSY}} + \sqrt{3}kQ \tag{15}$$

here the superscript SSY denotes the small scale yielding ($T = 0$) field in which the hoop stress directly ahead of the crack is $2.83\sigma_0$ while the corresponding Prandtl value is $2.97\sigma_0$. The small difference between the small scale yielding and the HRR stresses allows eqn (15) to be approximated as:

$$\sigma_m = \sigma_m^{\mathrm{HRR}} + \sqrt{3}kQ \tag{16}$$

The value of Q depends on the elastic wedge angle, and can be determined by combining eqns (14.4), (12.1) and (16):

$$Q = \left(\frac{\pi}{2} - 1 - \frac{2\varphi - \sin 2\varphi}{2 - \cos 2\varphi}\right) \Big/ \sqrt{3} \tag{17}$$

The complete stress field is then determined for the appropriate elastic wedge angle as already described. Figure 4 shows the variation of Q with the elastic wedge angle, φ, in the range $45^\circ \leqslant \varphi < 135^\circ$. When $\varphi = 45^\circ$, the stress distribution around the crack tip is identical to the fully constrained (HRR) field.

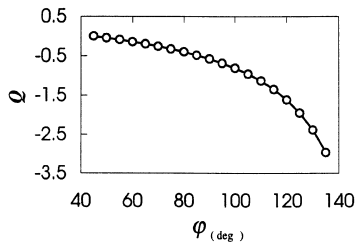

Fig. 4. The variation of the constraint parameter, Q, with elastic wedge angle.

Mixed Mode. Under mixed mode loading, comprising combinations of mode I and mode II, the nature of the remote elastic field can be defined by an elastic mixity parameter introduced by Shih (1974).

$$M_{el} = \frac{2}{\pi}\tan^{-1}\left(\frac{K_{\mathrm{I}}}{K_{\mathrm{II}}}\right) = \frac{2}{\pi}\tan^{-1}\left\{\lim_{r\to 0}\left[\frac{\sigma_{\theta\theta}(r,0)}{\sigma_{r\theta}(r,0)}\right]\right\} \tag{18}$$

The elastic mixity defines the ratio of tension to shear in the remote elastic field and also directly ahead of the crack in the fully elastic case. However when crack tip plasticity occurs, the ratio of tension to shear directly ahead of the crack is defined by a plastic mixity factor.

$$M_p = \frac{2}{\pi}\tan^{-1}\left\{\lim_{r\to 0}\left[\frac{\sigma_{\theta\theta}(r,0)}{\sigma_{r\theta}(r,0)}\right]\right\} \tag{19}$$

The elastic and plastic mixities are in general not identical. The mixed mode slip line fields under small scale yielding have been determined by Hancock et al. (1997) for compressible elastic deformation. The fields are closely similar to those determined in the present work which are illustrated in Fig. 5.

These fields can be understood by imagining that the constant stress sector ahead of the crack in mode I loading rotates as the mode II loading is applied and the elastic wedge on one crack flank expands. The slip line fields can be expressed in terms of the plastic mixity by noting that the plastic mixity defines the ratio of hoop to shear stress directly ahead of the crack. This can be determined by following the slip lines from a crack flank to the region directly ahead of the crack within the plastic region. Two possible conditions can be identified. In the first the fully plastic side of the crack comprises a constant stress triangle, a centred fan and part of a constant stress diamond, as illustrated in Fig. 6(a). In this case, the field is defined by the span of the centred fan, α, which is given by:

$$M_p = \frac{2}{\pi}\tan^{-1}\left(\frac{\cos 2\alpha - 1 - 2\alpha}{-\sin 2\alpha}\right) \quad \alpha \geqslant \pi/4 \tag{20}$$

Alternatively for lower values of mixity there may be two centred fans as illustrated in Fig. 6(b) in the fully plastic side. In this case a relation is established between the span of the two fans and the plastic mixity, while a second relation ensures that $(\alpha+\beta)$ is $\pi/4$. This allows the plastic mixity to be written as:

$$M_p = -\frac{2}{\pi}\tan^{-1}\left(\frac{\pi}{2} - 4\alpha - 1\right) \quad \alpha \leqslant \pi/4 \tag{21}$$

In the upper half of the configuration illustrated in Fig. 6(a), the field is fixed by the span of the elastic sector (φ) and the part span of the diamond (δ) where $\delta = \alpha - \pi/4$. Thus, φ and δ can be expressed in terms of the plastic mode.

$$M_p = \frac{2}{\pi}\tan^{-1}\left\{\frac{[\sin 2\delta + 2(\pi-\delta)](1-\cos 2\varphi) - 2\varphi + \sin 2\varphi}{\cos 2\delta(1-\cos 2\varphi)}\right\} \tag{22}$$

For low mixities, such as the configuration shown in Fig. 6(b), the upper half of the field comprises

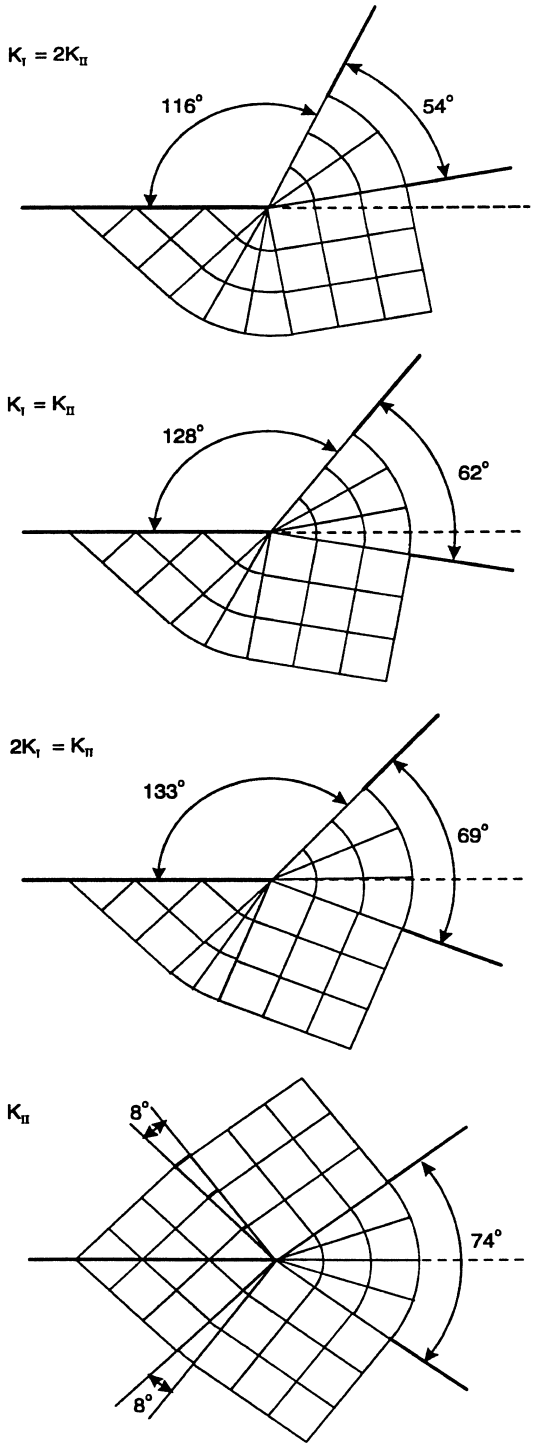

Fig. 5. Slip line fields with incomplete plasticity for mixed mode loading.

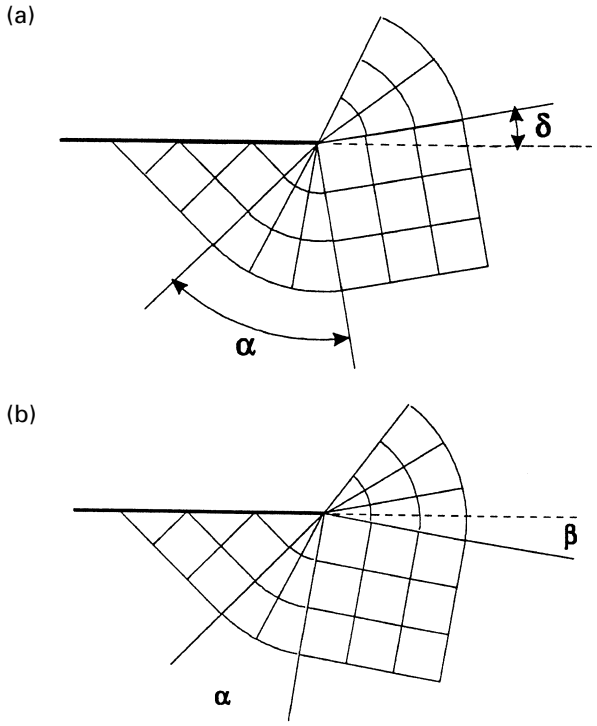

Fig. 6. Mixed mode slip line fields.

a centred fan and an elastic sector. This is fixed by the span of the elastic sector (ϕ) which can be given in terms of the plastic mixity.

$$M_p = \frac{2}{\pi}\tan^{-1}\left(2\pi - \frac{2\varphi - \sin 2\varphi}{1-\cos 2\varphi}\right) \tag{23}$$

For a given plastic mixity the stress field within the plastic sectors is defined from the Hencky equations. The sectors are thus fully defined in terms of the plastic mixity, and can be assembled to give full continuity of tractions. The fields for the four levels of mixity, listed in Table 1 including pure shear, have been analysed. The analytic solutions are shown in Fig. 7 where they will be compared with the finite element solutions.

3. Finite element solutions

To verify the analytical solutions, a finite element method has been used to obtain numerical solutions. Calculations have been performed in plane strain mode I loading with two levels of the T stress, $T = 0$ and $T/\sigma_0 = -0.443$. The Cartesian displacements (u_1, u_2) corresponding to the first two terms of the Williams expression are :

Table 1
Mode mixity for a range of mixed mode problems

	M_{el}	M_p
K_I	1.00	1.00
$K_I = 2K_{II}$	0.71	0.81
$K_I = K_{II}$	0.50	0.69
$K_I = 0.5K_{II}$	0.30	0.50
K_{II}	0.0	0.0

$$u_1 = u_1^K + u_1^T = \left(\frac{r}{2\pi}\right)^{1/2} \frac{K}{2G}\cos\frac{\theta}{2}\left[\eta - 1 + 2\sin^2\left(\frac{\theta}{2}\right)\right] + \frac{1+\eta}{8G} rT\cos\theta \tag{23.1}$$

$$u_2 = u_2^K + u_2^T = \left(\frac{r}{2\pi}\right)^{1/2} \frac{K}{2G}\sin\frac{\theta}{2}\left[\eta + 1 - 2\cos^2\left(\frac{\theta}{2}\right)\right] + \frac{\eta-3}{8G} rT\sin\theta \tag{23.2}$$

where $\eta = 3-4v$. G is the shear modulus and v is the Poisson's ratio. K and T are loading parameters established by the far field conditions.

The crack-tip fields for mode I and mixed mode problems have been modelled by using the highly focused mesh shown in Fig. 8. Symmetry allowed the mode I problem to be represented by a symmetric half. The mesh is based on 24 rings of 24 isoparametric second-order hybrid elements concentric with the crack tip. The crack tip thus consists of 49 initially coincident, but independent nodes. Displacement boundary conditions corresponding to eqns (23.1) and (23.2) were applied to the outer circumference of the mesh corresponding to nodal displacements associated with mode I and a compressive or zero T stress.

Mixed mode calculations have been performed under the levels of elastic mixity given in Table 1 where the corresponding levels of plastic mixity are also given. The corresponding boundary conditions have been applied to a full mesh around the crack tip as the mixed mode problem cannot be simplified by symmetry. The displacements, u_1 and u_2, corresponding to the K_I and K_{II} stress intensity factors have been applied on the outer boundary of the mesh.

$$u_1 = u_1^{K_I} + u_1^{K_{II}} = \left(\frac{r}{2\pi}\right)^{1/2} \frac{1}{2G}\left\{K_I\cos\frac{\theta}{2}\left[\eta - 1 + 2\sin^2\left(\frac{\theta}{2}\right)\right] + K_{II}\sin\frac{\theta}{2}\left[\eta + 1 + 2\cos^2\left(\frac{\theta}{2}\right)\right]\right\}$$

$$u_2 = u_2^{K_I} + u_2^{K_{II}} = \left(\frac{r}{2\pi}\right)^{1/2} \frac{1}{2G}\left\{K_I\sin\frac{\theta}{2}\left[\eta + 1 - 2\cos^2\left(\frac{\theta}{2}\right)\right] - K_{II}\cos\frac{\theta}{2}\left[\eta - 1 - 2\sin^2\left(\frac{\theta}{2}\right)\right]\right\} \tag{24}$$

In both the mode I and mixed mode cases, calculations were performed using ABAQUS (1995) with a non-hardening incompressible response. The stress field at the crack tip was determined by extrapolating the stress to the tip along radial lines such that the tip was approached asymptotically from different angles. These numerical solutions have been interpreted as slip line fields. Firstly,

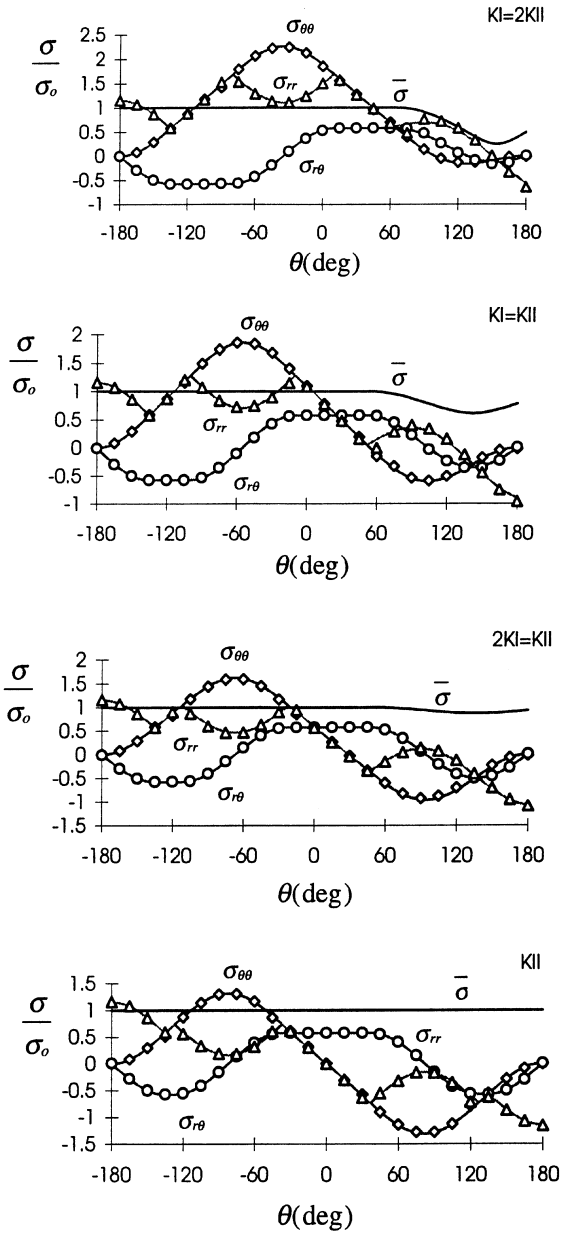

Fig. 7. The asymptotic stress distribution around a crack tip for mixed mode loading. The lines refer to the analytic solutions and the data points to the finite element solutions.

the angular span of the elastic sectors is determined from the angular range over which the yield criterion is not satisfied. Secondly, the span of the centred fan is determined from the angular range over which the mean stress varies linearly with angle within a plastic sector. Finally the

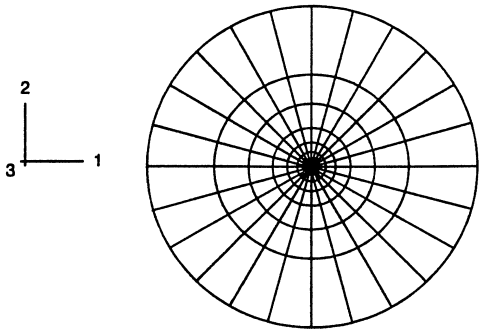

Fig. 8. Focused mesh.

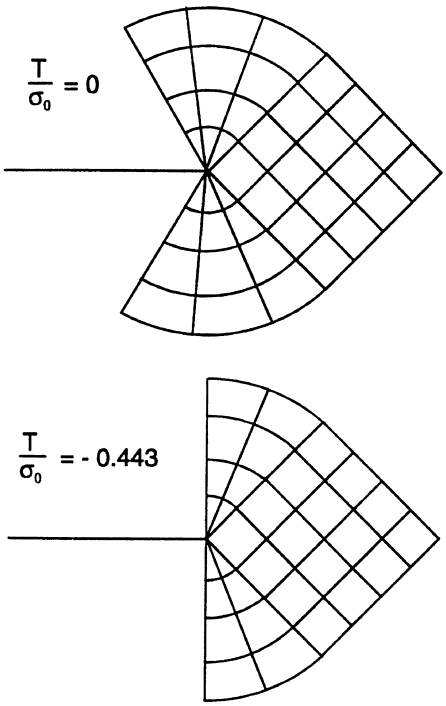

Fig. 9. Mode I slip line fields with incomplete plasticity.

constant stress sector is identified from the region in which the mean stress does not change with angle. These results are shown in the slip line fields of Fig. 9. The angular variation of each stress component and the Mises stress, under mode I, with $T = 0$ and $-0.443\sigma_0$, and in mixed mode loading are shown in Fig. 10 and Fig. 7. These numerical results are compared with the analytical solutions and it is clear that there is full agreement between the analytical solutions given by lines and the numerical solutions given as data points in both mode I and mixed mode loading.

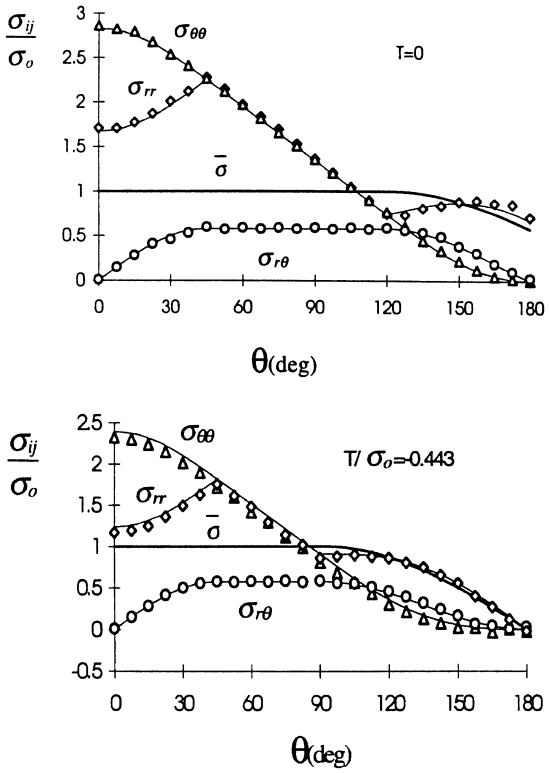

Fig. 10. The asymptotic stress distribution around a crack tip for mode I loading. The lines refer to the analytical solutions and the data points to the finite element solutions.

4. Conclusions

Analytical solutions for Mode I and mixed mode I/II fields have been constructed by using slip line solutions for plastic sectors and semi-infinite elastic wedge solutions for elastic sectors for incompressible plane strain deformation. The fields, which exhibit full continuity of tractions, have been verified by numerical calculations based on modified boundary layer formulations. Unlike the HRR fields, these fields do not exhibit plasticity at all angles around the crack tip. The difference between these fields and the HRR field can be attributed to the effect of higher order terms, which are significant even in small scale yielding ($T = 0$). In mode I, the HRR fields is identified as the complete Prandtl field, while in small scale yielding the Prandtl field is incomplete. Similarly in mixed-mode problems, the HRR fields exhibit plasticity at all angles around the crack tip (Shih, 1974), but the small scale yielding fields analysed in the present work exhibit incomplete plasticity except for the pure mode II case. Although analytic solutions for these fields have been assembled, it has not proved possible to establish an analytic relation between the inner elastic–plastic field and the outer elastic field, although this relationship has been established computationally.

In mode I the loss in constraint depends on the level of the compressive T stress which results in the formation of an elastic wedge on the crack flanks. The angular span of the elastic wedge

increases as T becomes more negative and corresponds to loss of constraint directly ahead of the crack tip. For a given value of the constraint parameter Q, the span of the elastic sector can be determined and the elastic and plastic sectors assembled around the crack tip to give the full analytic solution. These fields form the basis of a two parameter, constraint based characterization of mode I fields.

In mixed mode I/II fields the constant stress sector ahead of the mode I ($T = 0$) crack rotates with increasing mode II component, and loses constraint. Mixed mode fields near mode I consist of distortions of the mode I field in which the angular span of the crack flank elastic wedge increases with decreasing elastic mixity. Unlike the fields discussed by Shih (1974), these fields exhibit full continuity of tractions around the crack tip. Close to mode II, plasticity surrounds the crack tip, contact is established with the mixed mode HRR fields discussed by Shih (1974) and finally the mode II field discussed by Hutchinson is recovered.

Acknowledgements

J. Li acknowledges the support of an award from S.H.E.F.C. ABAQUS was made available by H.K.S. under academic licence. The authors thank the referees for pointing out the relevance of work by Nemat-Nasser and Obata (1984) of which the authors were unaware in the preparation of this paper.

References

ABAQUS V.5.4, 1994. ABAQUS Manual. Hibbit, Karlsson and Sorensen Inc., Providence, RI.

Betegón, C., Hancock, J.W., 1991. Two parameter characterisation of elastic–plastic crack tip fields. Journal of Applied Mechanics 58, 104–110.

Du, Z.-Z., Hancock, J.W., 1991. The effect of non-singular stresses on crack tip constraint. Journal of the Mechanics and Physics of Solids 39, 555–567.

Hancock, J.W., Reuter, W.A., Parks, D.M., 1993. Toughness and constraint parameterised by T. Constraint Effects in Fracture ASTM STP 1171, 121–140. American Society for Testing and Materials, Philadelphia, PA.

Hancock, J.W., Nekkal, A., Kartensen, A.D., 1997. Constraint effects in mixed mode loading. Proceedings of the Ninth International Conference on Fracture 4, 2015–2023.

Hill, R., 1950. The Mathematical Theory of Plasticity. Oxford University Press, Oxford.

Hutchinson, J.H., 1968a. Singular behaviour at the end of a tensile crack in a hardening material. Journal of the Mechanics and Physics of Solids 16, 13–31.

Hutchinson, J.H., 1968b. Plastic stress and strain fields at a crack tip. Journal of the Mechanics and Physics of Solids 16, 337–347.

Kirk, M.T., Koppenhoefer, K.C., Shih, C.F., 1993. Effect of constraint on dimensions needed to obtain structurally relevant toughness measures. Constraint effects in fracture. ASTM STP 1171, 79–103. American Society for Testing and Materials, Philadelphia, PA.

Larsson, S.G., Carlsson, A.J., 1973. Influence of non-singular terms on the specimen geometry on small scale yielding at a crack tip in elastic–plastic materials. International Journal of Fracture 19, 263–287.

Nemat-Nasser, S., Obata, M., 1984. On stress field near a stationary crack tip. Mechanics of Materials 3, 235–243.

O'Dowd, N.P., Shih, C.F., 1991a. Family of crack tip fields characterised by a triaxiality parameter : Part I—Structure of fields. Journal of the Mechanics and Physics of Solids 39, 939–963.

O'Dowd, N.P., Shih, C.F., 1991b. Family of crack tip fields characterised by a triaxiality parameter : Part II—Fracture applications. Journal of the Mechanics and Physics of Solids 39, 989–1015.

Rice, J.R., 1974. Limitations to the small scale yielding approximation for crack tip plasticity. Journal of the Mechanics and Physics of Solids 22, 17–26.
Rice, J.R., Rosengren, G.F., 1968. Plane strain deformation near a crack tip in a power law hardening material. Journal of the Mechanics and Physics of Solids 16, 1–12.
Rice, J.R., Tracey, D.M., 1973. Numerical and Computational Methods in Structural Mechanics. Academic Press, New York.
Shih, C.F., 1974. Small scale yielding analysis of mixed mode plane strain crack problems. Fracture Analysis, ASTM STP 560, 187–210.
Timoshenko, S.P., Goodier, J.N., 1970. Theory of Elasticity, 3rd edn. McGraw-Hill, New York.
Williams, M.L., 1957. On the stress distribution at the base of a stationary crack. Journal of Applied Mechanics 24, 111–114.
Zywicz, Z., Parks, D.M., 1990. Elastic–plastic analysis of frictionless contact at interfacial tips. International Journal of Fracture 42, 129–143.